Ultra-Low Loss and Flat Dispersion Circular Porous Core Photonic Crystal Fiber for Terahertz Waveguiding

Aboulwafa M. Singer [1,2], Ahmed M. Heikal [1,3], Hamdi A. El-Mikati [1], Salah S. A. Obayya [3*], and Mohamed Farhat O. Hameed [1,2,3*]

[1] Faculty of Engineering
Mansoura University, Mansoura 35516, Egypt

[2] Nanotechnology and Nanoelectronics Engineering Program
Zewail City of Science and Technology, October Gardens, 6th of October City, Giza 12578, Egypt
mfarahat@zewailcity.edu.eg

[3] Centre for Photonics and Smart Materials
Zewail City of Science and Technology, October Gardens, 6th of October City, Giza 12578, Egypt
sobayya@zewailcity.edu.eg

Abstract — A novel design of circular porous core photonic crystal fiber (CCPCF) is proposed and studied for Terahertz propagation with an ultra-low-loss. The effective index, effective mode area, dispersion, material and bending losses of the suggested design are studied using full vectorial finite element method. The CCPCF with high cladding air filling factor and porous core exhibits ultra-low material absorption loss of 0.022 cm^{-1} at a frequency of 1.0 THz. Further, very low bending losses of 2.2×10^{-18} cm^{-1} can be achieved for 1.0 cm bending radius at 1.0 THz with low confinement loss of 1.37×10^{-5} cm^{-1}. Additionally, an ultra-flat low dispersion of 0.61 ± 0.035 ps/THz/cm can be obtained within the frequency range of 0.8-1.0 THz. Therefore, the reported CCPCF has a strong potential for transmission in the Terahertz regime.

Index Terms — Bending losses, dispersion, photonic crystal fiber, porous core, terahertz waveguiding.

I. INTRODUCTION

Recently, THz photonic crystal fibers (PCFs) have granted a great interest in the scientific community because of their promising applications in telecommunication, medical science, spectroscopy, security, imaging, and sensing [1]–[7]. Currently, the THz waveguide is still under extensive research due to the material absorption losses. Additionally, there are some problems associated with transmitter-receiver alignment and atmosphere-dependent losses [8]. Therefore, long-distance communication in the THz regime is a big challenge. The PCF is suggested to overcome such high absorption losses. However, the solid core of PCF still absorbs an intolerable amount of the transmitted signal energy. The porous core with air holes is then introduced to PCF to reduce the effective material loss (EML) [9]–[11]. In this context, Bao *et al.* [12] have proposed a honeycomb terahertz fiber with an absorption loss of 1.5 cm^{-1} at 1.0 THz. Additionally, a hexagonal porous core PCF with an absorption loss of 0.17 cm^{-1} has been presented with Teflon as a background material [13]. Further, a porous core photonic bandgap fiber was proposed with EML of 0.432 cm^{-1} and dispersion loss of 2.5 ps/THz/cm [14]. Kaijage *et al.* [15] have also suggested an octagonal PCF for terahertz wave guidance with an EML of 0.070 cm^{-1} at f= 1.0 THz. In 2015, Islam *et al.* [16] have proposed a rotated hexagonal porous core single-mode fiber with an EML of 0.066 cm^{-1} and a core power fraction of 40%. Additionally, a circular cladding with a circular porous core was introduced [17] with an absorption loss of 0.053 cm^{-1}. A kagome lattice and hexagonal core were also reported [18] with EML of 0.034 cm^{-1}, low confinement loss at 1.0 THz frequency, and near-zero flattened dispersion of 0.60 ± 0.14 ps/THz/cm within the frequency range of 0.75-1.15 THz. However, the fabrication of kagome-structured fiber is more challenging than regular fiber with circular-shaped air holes. Islam *et al.*[19] have also presented a circular cladding with hexagonal porous core with an absorption loss of 0.053 cm^{-1}. Furthermore, hexagonal cladding PCF with a circular porous core was proposed with an absorption loss of 0.057 cm^{-1} [20]. Using the same structure, Islam *et al.* [1] have reduced the absorption loss to 0.043 cm^{-1}. An ultra-low loss hybrid porous core fiber was introduced for broadband applications [21] with small EML of 0.043 cm^{-1} and near-zero flattened dispersion properties.

In this paper, a novel design of PCF is reported for

Terahertz waveguiding with circular lattice and circular porous core. The geometrical parameters are studied to minimize the material, confinement and bending losses with a nearly zero and flat dispersion over the studied frequency range. The simulation results are obtained using the full vectorial finite element method (FVFEM) via the Comsol Multiphysics software package [22]. The suggested design has a very low absorption loss of 0.022 cm^{-1} at f= 1.0 THz with low confinement loss of 1.37×10^{-5} cm^{-1}. Further, the proposed PCF exhibits low bending loss and small flat dispersion of 0.61 $\pm$ 0.035 ps/THz/cm within the frequency range 0.8-1.0 THz. The achieved EML and bending loss are smaller than those introduced in the literature [1], [15]–[17], [19], [20], [23]–[29]. Further, the guiding properties of the proposed PCF are better than the previously reported circular PCF with EML of 0.053 cm^{-1}, confinement loss of 1×10^{-2} cm^{-1}, and dispersion of 1.23±0.09 ps/THz/cm [17].

The suggested PCF with low EML, confinement losses and bending losses can be used for telecommunication applications, medical spectroscopy and sensing purposes in the promising terahertz band. Additionally, the flat dispersion through the frequency range of 0.8-1.0 THz will offer an undegraded signal at the receiver terminal. This will in turn influence the speed and bandwidth of the transmitted signal.

II. DESIGN CONSIDERATIONS

The proposed CCPCF with the porous core is shown in Fig. 1. The cladding region consists of 8 successive rings of air holes. The first ring contains 10 holes with a diameter (d) of 90 μm. The total number of cladding air holes is 226. The spacing between two successive rings is called hole pitch (Λ) which depends directly on the cladding air filling factor (AFF). The AFF is the ratio between the hole diameter (d) and the hole pitch (Λ) which is kept constant at 0.96 to provide low effective material loss (EML). The second cladding ring holes' center is located at a distance of (d_{sc}) which depends on the hole pitch (Λ) and the core diameter (D_{core}). Therefore, (d_{sc}) could be changed automatically during the simulation with the core diameter and the hole pitch as well. In this study, $d_{sc}=(D_{core}/2)(1+\rho)+\Lambda$ where (ρ) is a constant factor. Therefore, we could obtain an explicit quasi TE mode and quasi TM mode as well [30]. The core has a diameter D_{core} of 460 μm and a total number of 37 holes whose diameter (d_{co}) depends directly on the porosity (P) of the core region. The porosity is the ratio between the total area of the air holes in the core region to the total core area [31]. In this study, 3 successive rings are used with 6, 12, and 18 air holes with hole pitch (Λ_{core}) of 66 μm. Additionally, a diameter $d_{co}=75.6P$ μm is used for the reported design. The background material is TOPAS with refractive index $n = 1.53$ and bulk material absorption loss $\alpha_{mat} = 0.2$ cm^{-1} at a frequency of 1.0 THz [15]. In this study, the effective index, EML, confinement losses, effective modal area, bending losses, fractional power, and dispersion of the quasi TE mode of the reported design are studied.
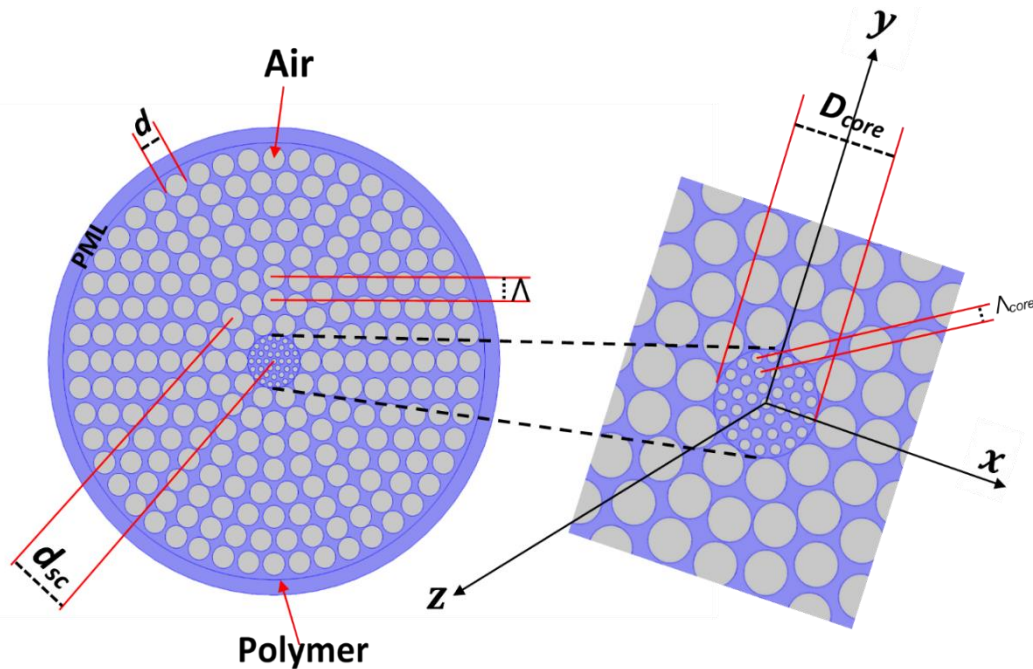

Fig. 1. Cross-section of the CCPCF with TOPAS as a background material.

III. NUMERICAL TECHNIQUE

The modal analysis of the suggested CCPCF is made by the full vectorial finite-element method (FVFEM) [32], [33] via the Comsol Multiphysics 5.2 commercial software package [22]. Starting from Maxwell's equations, the magnetic field-based vector wave equation can be obtained as:

$$\nabla \times (\varepsilon^{-1} \nabla \times H) - \omega^2 \mu_0 H = 0. \qquad (1)$$

where ω is the angular frequency, and μ_0 is the free space permeability. Further, $\varepsilon = \varepsilon_0 \varepsilon_r$ is the permittivity of the waveguide material where ε_0 is the free space permittivity and ε_r is the relative permittivity of the waveguide material. The following eigenvalue equation can be obtained by applying the standard finite element method (FEM) procedure to equation (1):

$$[K]\{H\} - \beta^2[M]\{H\} = \{0\}. \qquad (2)$$

where [K] and [M] are the global stiffness and mass matrices, [H] is the global magnetic field vector, {0} is the null vector and β is the propagation constant. The eigenvalue equation can be solved to obtain the eigenvector H and the corresponding eigenvalue β. Additionally, the effective index of the propagation mode is calculated from β since $N_{eff} = \beta/k$, where k is the free space wavenumber.

Through the modal analysis, a set of modes is calculated by the FVFEM and the dominant mode is defined as the mode with the highest real effective index value. Since $\nabla . H = 0$ and interface boundary conditions are automatically satisfied in the formulation, then there is no chance for spurious (nonphysical) modes to appear in the spectrum of the solution. The cross-section of the waveguide structure is discretized using the VFEM. In this study, a minimum mesh element size of 1.19 μm is taken with a total number of degrees of freedom of 640381, with 65748 total number of elements. Additionally, A circular-shaped perfectly-matched layer is employed to calculate the leakage loss of the studied modes. An Intel Core i5 computer processor at 2.5 GHz with 8.0 GB RAM and 64-bit operating system was utilized to run the software with an average runtime of 89 seconds per run.

IV. RESULTS AND DISCUSSION

In order to calculate the confinement losses accurately, the PML thickness is studied. Figure 2 shows the confinement losses variation with the PML radius-to-cladding radius ratio. It may be seen from this figure that the confinement losses of the quasi TE and TM modes are nearly constant at 1.37×10^{-5} cm^{-1} and 3.65×10^{-6} cm^{-1} at a ratio of 1.03 and $f = 1.0$ THz. Therefore, the PML radius is kept at 1.07 of the cladding radius throughout the whole study.

Figure 3 shows the frequency-dependent effective index N_{eff} of the fundamental quasi TE and quasi TM modes of the CCPCF for three porosity cases 20%, 30%, and 40% in the Terahertz range of 0.8-1.3 THz. It may be seen that N_{eff} increases with increasing the frequency

while it decreases with the porosity of the core region. As the frequency increases, the confinement of the light through the core region increases which increases the effective index of the supported modes. Further, the leakage of the mode toward the cladding region increases by increasing the porosity percentage as may be seen in the field plot in Fig. 3. Therefore, the maximum porosity of 40% has been used. If the porosity is further increased, the distance between the adjacent holes becomes small which will be a challenge for the fabrication process. Additionally, the mode will have high leakage to the cladding region which increases the confinement losses. As a result, the effective index of the quasi TE and TM modes decreases by increasing the porosity percentage as shown in Fig. 4. Further, the effective index of the quasi TE mode at a specific porosity percentage is very close to that of the quasi TM mode due to the symmetry of the proposed design.
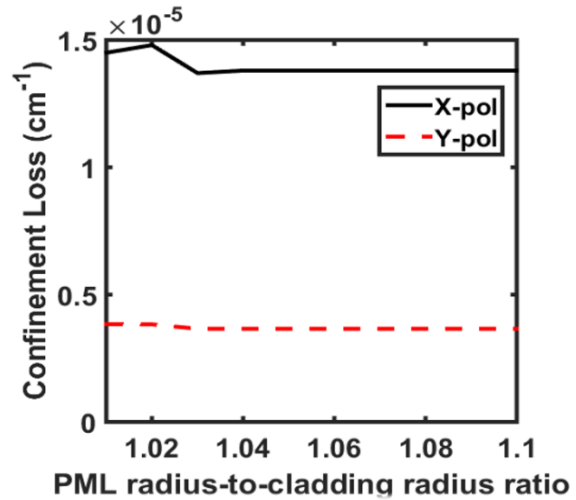

Fig. 2. Confinement loss of the quasi TE/TM mode versus the PML radius-to-cladding radius ratio.

The effective material loss (EML) α_{eff} could be considered as the main factor of the power dissipation in the THz band and can be calculated by the expression [34]:

$$\alpha_{eff} = \frac{\sqrt{\varepsilon_0/\mu_0} \int_{mat} n_{mat}|E|^2 \alpha_{mat} dA}{|\int_{all} S_z \, dA|}. \qquad (3)$$

where n_{mat} is the material refractive index, α_{mat} is the bulk material absorption loss, ε_0 and μ_0 are the permittivity and permeability of the free space, respectively, and S_z is the z-component of the pointing vector defined as $S_z = \frac{1}{2}(E \times H).z$. The EML of the proposed fiber for different porosity values 20%, 30%, and 40% is shown in Fig. 5. It may be seen that the EML decreases by increasing the porosity percentage. The figure depicts that the EML values have a maximum of 0.031 cm^{-1} at a porosity of 20% at $f = 1.3$ THz and a minimum of 0.021 cm^{-1} at a porosity of 40% at $f = 0.8$

THz. At the operating frequency of 1.0 THz, the EML is equal to 0.022 cm^{-1} which is far better than those reported in Table 1. If a frequency of 0.8 THz is used, the EML will not exceed $\approx$ 0.021 cm^{-1}. Therefore, the proposed design is highly qualified for many Terahertz applications. The high density of the cladding air holes and the porosity of the core region are responsible for achieving low EML. This is due to the reduced amount of the bulk material in the whole design, especially through the core region.
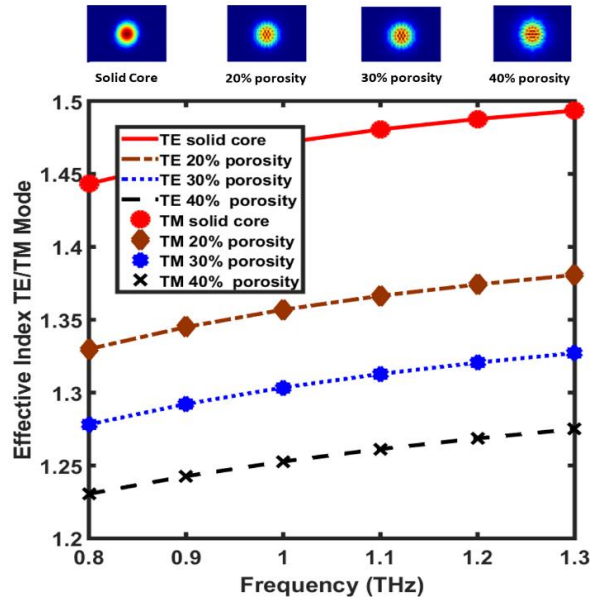

Fig. 3. The effective index of the fundamental quasi TE/TM mode versus the frequency at different porosity percentages. The inset shows the main electric field component of the quasi TM mode at different porosities.
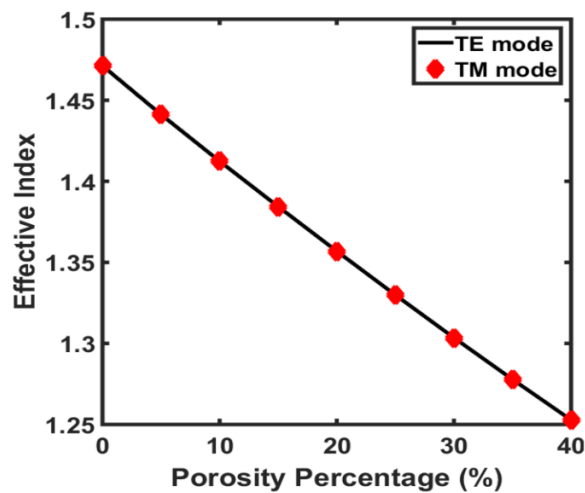

Fig. 4. The effective index of the fundamental quasi TE and quasi TM modes versus the porosity percentage (%).
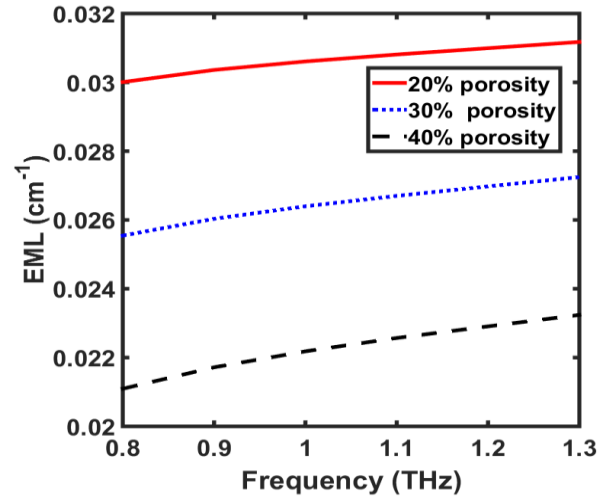

Fig. 5. EML versus the operating frequency at different porosity percentages.

The confinement loss of the supported modes is also implemented as given by [35]–[37]:

$$L_c = 8.686 \, K_0 \, Im \, (N_{eff}). \qquad (4)$$

where K_0 is the propagation constant of free space and $Im(N_{eff})$ is the imaginary part of the effective index N_{eff} of the studied mode. Figure 6 shows the calculated confinement loss of the quasi TE mode supported by the proposed CCPCF versus the frequency at different porosity percentages. The mode field starts to leak out the core region by increasing the porosity percentage which increases the confinement losses. Additionally, as the frequency increases, the confinement of the mode through the core region increases. Further, the confinement losses are smaller than the material loss with a value of $1.37 \times 10^{-5} \, cm^{-1}$ at f= 1.0 THz and porosity of 40%. Therefore, the confinement losses can be neglected if compared to the material loss. It may be seen that the proposed structure enjoys a low confinement loss due to the high AFF value of the cladding. Therefore, a high index contrast is obtained between the cladding and the core regions with better field confinement in the core region.

The effective modal area (A_{eff}) of the quasi TE mode of the proposed CCPCF is also analyzed through the frequency band of 0.8-1.3 THz. The A_{eff} could show the mode confinement through the core region and is given by [1], [10],[37]:

$$A_{eff} = \frac{[\int I(r)rdr]^2}{\int I^2(r)rdr}. \qquad (5)$$

where $I(r) = |E_t|^2$ is the transverse electric field intensity distribution in the fiber cross-section. Figure 7 shows the variation of the frequency-dependent effective mode area of the quasi TE mode. It is evident from this figure that the effective mode area is proportional to the porosity percentage and is inversely proportional to the operating frequency. This is due to the good confinement

of the studied mode at high frequency and small porosity. The effective mode area at 1.0 THz and 40% porosity is equal to $1.22 \times 10^5 \ \mu m^2$, which is very comparable to most of the reported values in Table 1.
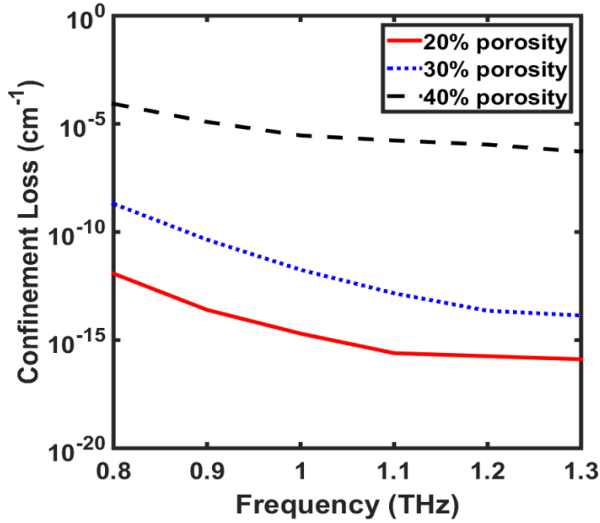

Fig. 6. Frequency-dependent confinement loss of the quasi TE mode at different porosity percentages.
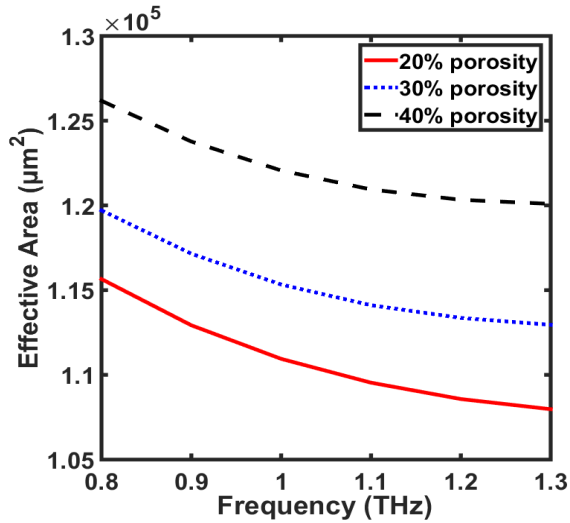

Fig. 7. Frequency-dependent effective mode area of the quasi TE mode at different porosity percentages.

The PCFs can also suffer from bending losses (α_{BL}) which can lead to the distortion of the optical mode. The α_{BL} can be expressed as [38]:

$$\alpha_{BL} \cong \left(\frac{\sqrt{\pi}}{8A_{eff}}\right)\left(\frac{1}{\beta(\beta^2-\beta_{cl}^2)^{\frac{1}{4}}}\right)\left(\frac{exp\left(-\frac{2}{3}R_b(\beta^2-\beta_{cl}^2)^{\frac{3}{2}}\beta^{-2}\right)}{\sqrt{R_b(\beta^2-\beta_{cl}^2)\beta^{-2}+R_c}}\right). \quad (6)$$

where β is the propagation constant as $\beta = 2\pi N_{eff}/\lambda$, R_c is the fiber core radius and R_b is the bending radius. In this study, it is assumed that the cladding refractive

index is approximately unity due to the high filling factor of the cladding region. Further, β_{cl} is calculated for each frequency as $\beta_{cl} = 2\pi \times 1/\lambda$. Figure 8 shows the frequency-dependent α_{BL} at different porosity percentages. It may be seen that the bending losses increase with increasing the porosity while it decreases with increasing the frequency. This is due to the good confinement of the light through the core region at high frequency. Higher bending loss of $1.96 \times 10^{-13} cm^{-1}$ is achieved at $f = 0.8$ THz and porosity of 40%. However, a small value of $1.0 \times 10^{-37} cm^{-1}$ is obtained at a frequency of 1.3 THz and a porosity of 20%. The bending loss at $f = 1.0$ THz is equal to $2.2 \times 10^{-18} \ cm^{-1}$ with a porosity of 40%.
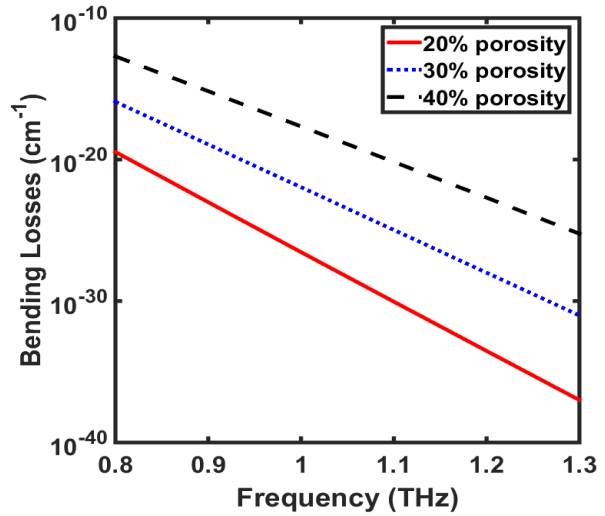

Fig. 8. Frequency-dependent bending loss of the quasi TE mode at different porosity percentages.

It is aimed to maximize the traveled power through the porous core region for efficient THz regime transmission. Therefore, we calculated the fractional propagated power through the proposed CCPCF using the expression [39], [40]:

$$\varphi = \frac{\int_{core} S_z \ dA}{\int_{all} S_z \ dA}. \quad (7)$$

where the numerator represents the integration of the z-component of the pointing vector over the core holes only while the denominator shows the integration all over the whole design. Figure 9 shows the fractional power of the quasi TE mode through the proposed CCPCF versus the frequency at different porosity percentages. The figure shows that high fractional power of 41.7% is achieved at $f = 1.3$ THz and porosity of 40%. Further, a fractional power of 41.16% is obtained at f=1.0 THz and porosity of 40%, which is a relatively high ratio. It should be also noted that the proposed CCPCF provides a nearly constant fractional power at low porosity value (20% and 30%) through the frequency

range of 0.8-1.3 THz which increases accordingly with the porosity percentages.

Next, the dispersion characteristics of the proposed CCPCF are analyzed. It is worth noting that the refractive index of the TOPAS material is nearly constant in the frequency range of 0.1-1.5 THz where the material dispersion can be totally neglected [12]. Then, the waveguide dispersion is only analyzed. The dispersion coefficient (β_2) can be calculated by [41]:

$$\beta_2 = \frac{1}{c}\left(2\frac{dN_{eff}}{d\omega} + \omega\frac{d^2N_{eff}}{d\omega^2}\right). \qquad (8)$$

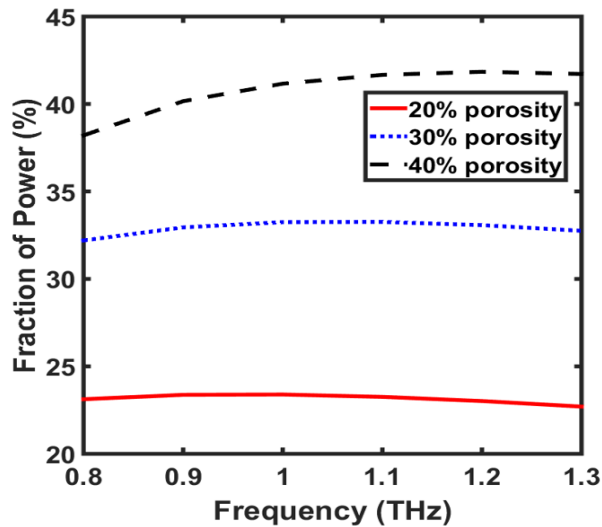where $\omega = 2\pi f$ is the radial frequency.

Fig. 9. The fraction of power percentage of the quasi TE mode through the core holes versus the frequency at different porosity percentages.
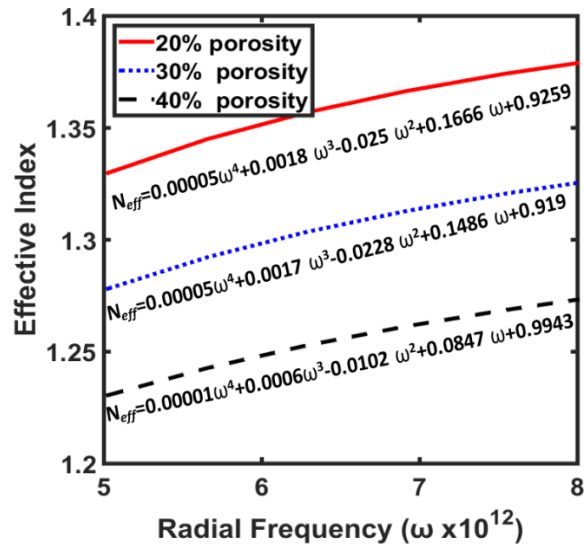

Fig. 10. The effective index N_{eff} of the quasi TE mode versus the radial frequency.

Figure 10 shows the relationship between N_{eff} and ω for three different porosity percentages as derived using the least square method (LSM) with a polynomial of the fourth order. The three equations have been mathematically differentiated and applied to the formula in Eq. (8). Figure 11 shows the frequency-dependent dispersion of the quasi TE mode of the proposed CCPCF for the three porosity cases. The average dispersion in the range of 0.8-1.3 THz is 0.15±0.13 ps/THz/cm for 20% porosity, 0.12±0.05 ps/THz/cm for 30% porosity and 0.97 ± 0.39 ps/THz/cm for 40% porosity. It may be also seen from Fig. 11 that at 40% porosity, the maximum value of dispersion is 1.36 ps/THz/cm at 1.3 THz and the minimum value is 0.58 ps/THz/cm at 0.9 THz (both are very small). It should be also noted that the proposed CCPCF has a nearly zero flat dispersion in the frequency range of 0.8-1.0 THz with an average value of 0.61±0.035 ps/THz/cm at 40% porosity. Such a very small dispersion is obtained over a wide range of frequencies which is very comparable to those reported in Table. 1. The calculated dispersion is directly related to the effective index N_{eff} of the supported modes. Such modes are confined through the porous core and the innermost cladding air holes. Therefore, the N_{eff} and hence the dispersion can be controlled by the geometrical parameters of the PCF.
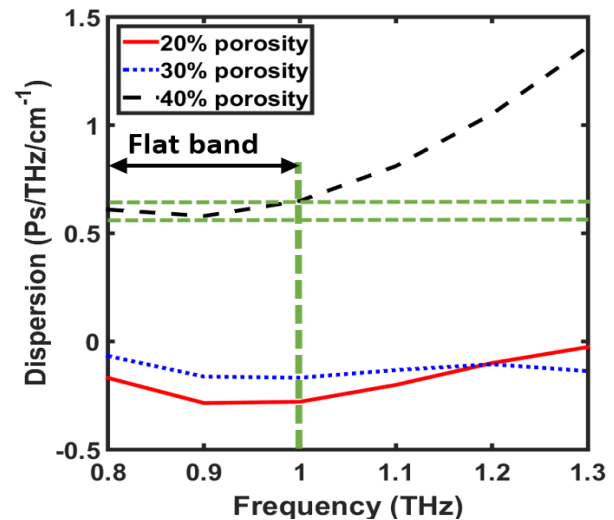
Fig. 11. The frequency dependent dispersion β_2 at different porosity percentages.

The proposed design can be fabricated using the most common stack-and-draw method [42]. Our proposed CCPCF is assumed to be simple-to-stack as the whole structure enjoys a high degree of symmetry around the center of the core with relatively low core porosity percentages. Therefore, the stacking process will be easy and will provide a high degree of accuracy by the end of the drawing process.

A comparison between the proposed CCPCF and the previously-published PCF for THz guiding is shown in Table 1. It is revealed from this table that the proposed CCPCF has better comprehensive characteristics than those reported previously. The suggested design has EML of 0.022 cm^{-1} at f = 1.0 THz while the other PCFs have EML within the range from 0.034 to 0.070 cm^{-1}. Further, the confinement loss of the CCPCF of $1.37 \times 10^{-5} cm^{-1}$ which is very comparable to all of the mentioned papers including [23], [24], and [25]. It is also noticed that the obtained effective mode area has a value of $1.22 \times 10^{5} \mu m^{2}$ which is also very comparable to the previous results. The bending loss of the suggested design is only 0.2% of the minimum achieved result [20] as shown in Table 1. The fractional power is also comparable to the other values [27] with a nearly constant value over the studied frequency range of 0.8-1.3 THz at porosity percentages of 20% and 30%. Further, an ultra-flattened nearly zero dispersion of (0.61 ± 0.035 Ps/THz/cm) is achieved over a frequency range from 0.8 to 1.0 THz which is very comparable to the minimum dispersion of (0.14 ± 0.07Ps/THz/cm) reported in [23]. Therefore, the proposed design would be an efficient transmission structure for the THz regime. It may be noted that the suggested

design has overall better guiding characteristics at the same time than those reported in the literature as shown in Table 1. However, short manufacture length and high price are the main disadvantages of using PCF as transmission media for telecommunications in THz regime. Additionally, the coupling of PCF with with other waveguides and devices is not straight forward.

V. CONCLUSION

In this paper, we proposed a CCPCF for the THz regime with an ultra-low EML of 0.022 cm^{-1}, low confinement losses of1.37×10^{-5} cm^{-1} and low bending losses of 2.2×10^{-18} cm^{-1} at 1.0 THz. Further, a wide-band flat low dispersion of 0.61 ± 0.035 ps/THz/cm is achieved within the frequency range of 0.8-1.0 THz. The structure has almost a constant fractional power for each porosity percentage through the frequency range of 0.8-1.3 THz with a comparable value of 41.16% at 1.0 THz. The reported CCPCF has a superior guiding mechanism than the previous circular PCF [17] with EML of 0.053 cm^{-1}, a confinement loss of 1×10^{-2} cm^{-1}, and dispersion of 1.23 ± 0.09 ps/THz/cm. Therefore, the reported CCPCF has a strong potential for transmission in the Terahertz regime.

Table 1: A comparison between the CCPCF and the previously published papers

Structure	Year	EML (cm^{-1}) at f =1.0 THz	Confinement Losses (cm^{-1}) at f =1.0 THz	Effective Mode Area (μm^{2}) at f =1.0 THz	Bending Losses (cm^{-1}) at f =1.0 THz	Fraction of Power (%) at f =1.0 THz	Dispersion (Ps/THz/cm)	Flat Dispersion Bandwidth (THz)
CCPCF		0.022	1.37×10^{-5}	1.22×10^{5}	2.2×10^{-18}	41.16	0.61 ± 0.035	0.8-1.0
[23]	2019	0.062	4.7×10^{-7}	------------	------------	-----------	0.14 ± 0.07	0.6-0.85
[26]	2019	0.07	1.66×10^{-3}	9×10^{4}	2.61×10^{-14}	-----------	1.2 ± 0.32	1.1-1.9
[27]	2019	0.04	1×10^{-4}	1.65×10^{5}	------------	40	0.98 ± 0.09	1.0-2.0
[24]	2018	0.065	3.8×10^{-9}	1.8×10^{5}	------------	-----------	1.3 ± 0.03	1.0-1.8
[25]	2018	0.05	1×10^{-9}	------------	------------	-----------	0.53 ± 0.07	0.5-1.48
[1]	2017	0.043	$1 \times 10^{-2.5}$	2.1×10^{5}	------------	47	1.14 ± 0.09	1.0-1.3
[20]	2017	0.057	6.9×10^{-3}	1.1×10^{5}	1.07×10^{-15}	42	1.3 ± 0.55	0.7-1.2
[28]	2017	0.034	$1 \times 10^{-3.7}$	6×10^{5}	------------	44	0.94 ± 0.09	0.7-1.3
[19]	2016	0.053	6.3×10^{-4}	------------	------------	47	1.2 ± 0.25	1.0-1.55
[17]	2015	0.053	1×10^{-2}	------------	------------	46	1.23 ± 0.09	0.9-1.3
[16]	2015	0.066	4.73×10^{-4}	------------	$\approx 1.310^{-12}$	40	1.06 ± 0.12	0.5-1.08
[15]	2013	0.070	1×10^{-1}	1.5×10^{5}	1.2×10^{-9}	-----------	---------------	-----------
[29]	2011	0.042	------------	1.04×10^{5}	-----------	50	≈ 3 with 0.0373 ps m^{-1} μm^{-1} SD	-----------

REFERENCES

[1] M. S. Islam, *et al.*, "Extremely low material loss and dispersion flattened TOPAS based circular porous fiber for long distance terahertz wave transmission," *Optical Fiber Technology*, vol. 34, pp. 6-11, 2017.

[2] Q. Chen, Z. Jiang, G. X. Xu, and X.-C. Zhang, "Near-field terahertz imaging with a dynamic aperture," *Optics Letters*, vol. 25, no. 15, pp. 1122-1124, 2000.

[3] H. Thenmozhi, M. M. Rajan, V. Devika, D. Vigneswaran, and N. Ayyanar, "D-glucose sensor using photonic crystal fiber," *Optik*, vol. 145, pp. 489-494, 2017.

[4] S. Chowdhury, S. Sen, K. Ahmed, and S. Asaduzzaman, "Design of highly sensible porous shaped photonic crystal fiber with strong confinement field for optical sensing," *Optik*, vol. 142, pp. 541-549, 2017.

[5] M. S. Islam, J. Sultana, A. Dinovitser, K. Ahmed,

B. W.-H. Ng, and D. Abbott, "Sensing of toxic chemicals using polarized photonic crystal fiber in the terahertz regime," *Optics Communications*, vol. 426, pp. 341-347, 2018.

[6] M. S. Islam, J. Sultana, A. A. Rifat, A. Dinovitser, B. W.-H. Ng, and D. Abbott, "Terahertz sensing in a hollow core photonic crystal fiber," *IEEE Sensors Journal*, vol. 18, no. 10, pp. 4073-4080, 2018.

[7] M. S. Islam, *et al.*, "A novel approach for spectroscopic chemical identification using photonic crystal fiber in the terahertz regime," *IEEE Sensors Journal*, vol. 18, no. 2, pp. 575-582, 2017.

[8] Z. Zhang, *et al.*, "Research on terahertz photonic crystal fiber characteristics with high bire-fringence," *Optik-International Journal for Light and Electron Optics*, vol. 125, no. 1, pp. 154-158, 2014.

[9] F. Poli, A. Cucinotta, and S. Selleri, *Photonic Crystal Fibers: Properties and Applications*. vol. 102. Springer Science & Business Media, 2007.

[10] Z. Frederic, R. Gilles, and N. Andre, *Foundations of Photonic Crystal Fibres*. World Scientific, 2005.

[11] M. Skorobogatiy and J. Yang, *Fundamentals of Photonic Crystal Guiding*. Cambridge University Press, 2009.

[12] H. Bao, K. Nielsen, H. K. Rasmussen, P. U. Jepsen, and O. Bang, "Fabrication and characterization of porous-core honeycomb bandgap THz fibers," *Optics Express*, vol. 20, no. 28, pp. 29507-29517, 2012.

[13] M. Uthman, B. M. A. Rahman, N. Kejalakshmy, A. Agrawal, and K. T. V. Grattan, "Design and characterization of low-loss porous-core photonic crystal fiber," *IEEE Photonics Journal*, vol. 4, no. 6, pp. 2315-2325, 2012.

[14] J. Liang, L. Ren, N. Chen, and C. Zhou, "Broadband, low-loss, dispersion flattened porous-core photonic bandgap fiber for terahertz (THz)-wave propagation," *Optics Commun-ications*, vol. 295, pp. 257-261, 2013.

[15] S. F. Kaijage, Z. Ouyang, and X. Jin, "Porous-core photonic crystal fiber for low loss terahertz wave guiding," *IEEE Photonics Technology Letters*, vol. 25, no. 15, pp. 1454-1457, Aug. 2013, doi: 10.1109/LPT.2013.2266412.

[16] R. Islam, G. K. M. Hasanuzzaman, M. S. Habib, S. Rana, and M. A. G. Khan, "Low-loss rotated porous core hexagonal single-mode fiber in THz regime," *Optical Fiber Technology*, vol. 24, pp. 38-43, 2015.

[17] R. Islam and S. Rana, "Dispersion flattened, low-loss porous fiber for single-mode terahertz wave guidance," *Optical Engineering*, vol. 54, no. 5, p. 055102, 2015.

[18] G. K. M. Hasanuzzaman, M. S. Habib, S. A. Razzak, M. A. Hossain, and Y. Namihira, "Low loss single-mode porous-core kagome photonic crystal fiber for THz wave guidance," *Journal of Lightwave Technology*, vol. 33, no. 19, pp. 4027-4031, 2015.

[19] M. S. Islam, S. Rana, M. R. Islam, M. Faisal, H. Rahman, and J. Sultana, "Porous core photonic crystal fibre for ultra-low material loss in THz regime," *IET Communications*, vol. 10, no. 16, pp. 2179-2183, 2016.

[20] M. A. Habib and M. S. Anower, "A novel low loss porous-core photonic crystal fiber for terahertz wave transmission," in *2017 Inter-national Conf-erence on Electrical, Computer and Communication Engineering (ECCE)*, pp. 56-59, 2017.

[21] M. S. Islam, J. Sultana, J. Atai, D. Abbott, S. Rana, and M. R. Islam, "Ultra low-loss hybrid core porous fiber for broadband applications," *Applied Optics*, vol. 56, no. 4, pp. 1232-1237, 2017.

[22] COMSOL: Multiphysics Software for Optimizing Designs, *COMSOL Multiphysics*®. https://www.comsol.com/ (accessed Jan. 20, 2020).

[23] S. Mei, *et al.*, "Suspended graded-index porous core POF for ultra-flat near-zero dispersion terahertz transmission," *Optical Fiber Technology*, vol. 52, p. 101946, 2019.

[24] M. S. Islam, *et al.*, "A modified hexagonal photonic crystal fiber for terahertz applications," *Optical Materials*, vol. 79, pp. 336-339, 2018.

[25] J. Sultana, *et al.*, "Highly birefringent elliptical core photonic crystal fiber for terahertz application," *Optics Communications*, vol. 407, pp. 92-96, Jan. 2018, doi: 10.1016/j.optcom. 2017.09.020.

[26] M. A. Habib and M. S. Anower, "Design and numerical analysis of highly birefringent single mode fiber in THz regime," *Optical Fiber Tech-nology*, vol. 47, pp. 197-203, 2019.

[27] J. Sultana, M. R. Islam, M. Faisal, K. M. A. Talha, and M. S. Islam, "Design and analysis of a Zeonex based diamond-shaped core kagome lattice photonic crystal fiber for T-ray wave transmission," *Optical Fiber Technology*, vol. 47, pp. 55-60, 2019.

[28] M. S. Islam, J. Sultana, J. Atai, M. R. Islam, and D. Abbott, "Design and characterization of a low-loss, dispersion-flattened photonic crystal fiber for terahertz wave propagation," *Optik*, vol. 145, pp. 398-406, 2017.

[29] J. J. Bai, J. N. Li, H. Zhang, H. Fang, and S. J. Chang, "A porous terahertz fiber with randomly distributed air holes," *Applied Physics B*, vol. 103, no. 2, pp. 381-386, 2011.

[30] S. Liang, *et al.*, "Influences of asymmetrical geometric structures on the birefringence of index-guiding photonic crystal fiber," *Optik*, vol. 180, pp. 973-983, 2019.

[31] M. H. Muhammad, M. F. O. Hameed, A. M.

Heikal, and S. S. Obayya, "Porous core photonic crystal fibre with metal-coated central hole for terahertz applications," *IET Optoelectronics*, vol. 9, no. 2, pp. 37-42, 2015.

[32] S. S. A. Obayya, B. M. A. Rahman, and H. A. El-Mikati, "New full-vectorial numerically efficient propagation algorithm based on the finite element method," *Journal of Lightwave Technology*, vol. 18, no. 3, p. 409, 2000.

[33] S. S. A. Obayya, B. M. A. Rahman, K. T. V. Grattan, and H. A. El-Mikati, "Full vectorial finite-element-based imaginary distance beam propagation solution of complex modes in optical waveguides," *J. Lightwave Technol., JLT*, vol. 20, no. 6, p. 1054, June 2002.

[34] A. W. Snyder and J. Love, *Optical Waveguide Theory*. Springer Science & Business Media, 2012.

[35] S. F. Kaijage, *et al.*, "Broadband dispersion compensating octagonal photonic crystal fiber for optical communication applications," *Jpn. J. Appl. Phys.*, vol. 48, no. 5R, p. 052401, May 2009, doi: 10.1143/JJAP.48.052401.

[36] Y. E. Monfared, A. R. Maleki Javan, and A. R. Monajati Kashani, "Confinement loss in hexagonal lattice photonic crystal fibers," *Optik*, vol. 124, no. 24, pp. 7049-7052, Dec. 2013, doi: 10.1016/j.ijleo.2013.05.168.

[37] A. Medjouri, L. M. Simohamed, O. Ziane, and A. Boudrioua, "Analysis of a new circular photonic crystal fiber with large mode area," *Optik*, vol. 126, no. 24, pp. 5718-5724, Dec. 2015, doi: 10.1016/j.ijleo.2015.09.035.

[38] M. D. Nielsen, N. A. Mortensen, M. Albertsen, J. R. Folkenberg, A. Bjarklev, and D. Bonacinni, "Predicting macrobending loss for large-mode area photonic crystal fibers," *Opt. Express, OE*, vol. 12, no. 8, pp. 1775-1779, Apr. 2004, doi: 10.1364/OPEX.12.001775.

[39] N. Chen, J. Liang, and L. Ren, "High-birefringence, low-loss porous fiber for single-mode terahertz-wave guidance," *Applied Optics*, vol. 52, no. 21, pp. 5297-5302, 2013.

[40] Y. Hou, F. Fan, Z.-W. Jiang, X.-H. Wang, and S.-J. Chang, "Highly birefringent polymer terahertz fiber with honeycomb cladding," *Optik - International Journal for Light and Electron Optics*, vol. 124, no. 17, pp. 3095-3098, Sep. 2013, doi: 10.1016/j.ijleo.2012.09.040.

[41] X. Tang, *et al.*, "Elliptical hollow fiber with inner silver coating for linearly polarized terahertz transmission," *IEEE Photonics Technology Letters*, vol. 25, no. 4, pp. 331-334, 2013.

[42] D. M. Chow, S. R. Sandoghchi, and F. R. M. Adikan, "Fabrication of photonic crystal fibers," in *2012 IEEE 3rd International Conference on Photonics*, pp. 227-230, Oct. 2012, doi: 10.1109/ICP.2012.6379830.